Advanced Quantum Technologies

ADVANCED QUANTUM TECHNOLOGIES
www.advquantumtech.com

ARTICLE

The Effect of Gravity on Continuous-Variable Multiparty Quantum Communication

Liangqi Zheng[1] | Jian Zhou[1] | Jinjing Shi[2] | Ying Guo[3] | Guangqiang He[4]

[1]College of Computer Science and Mathematics, Central South University of Forestry and Technology, Changsha, P. R. China | [2]School of Electronic Information, Central South University, Changsha, P. R. China | [3]School of Computer Science, Beijing University of Posts and Telecommunications, Beijing, P. R. China | [4]State Key Laboratory of Advanced Optical Communication Systems and Networks, Department of Electronic Engineering, Shanghai Jiao Tong University, Shanghai, P. R. China

Correspondence: Jian Zhou (13142153489@163.com)

Received: 10 February 2026 | **Revised:** 31 March 2026 | **Accepted:** 17 April 2026

Keywords: continuous-variable multiparty quantum communications | gravitational effects | non-inertial accelerations | quantum communication complexities | quantum secret sharing protocols

ABSTRACT

Quantum communication is gradually shifting from terrestrial fiber-optic communication to satellite-based space communication. The impact of gravitational fields on quantum states in quantum communication protocols cannot be overlooked. In this paper, a general method to investigate how non-inertial motion affects multiparty quantum communication is proposed. Specifically, we examine the influence of non-inertial motion on the performance of the protocol based on measurement-device-independent multiparty quantum communication using continuous-variable Greenberger–Horne–Zeilinger (CV GHZ) states. Our results demonstrate that the choice of system configuration and cryptographic scheme largely determines the effects of gravitational fields.

1 | Introduction

Multiparty quantum communication refers to a communication method that realizes secure information transmission and key sharing among three or more nodes based on quantum mechanics principles [1, 2]. It encompasses two typical schemes, namely quantum cryptography conference (QCC) [3] and quantum secret sharing (QSS) [4, 5]. In the QCC, every member within a group can access encrypted messages disseminated by other group members, while non-members are strictly prohibited from accessing this information. In the QSS, authorized members of a conferencing group can collaboratively decrypt encrypted messages sent by any group member, whereas unauthorized individuals cannot retrieve the information through any form of collaboration. The CV MDI multiparty quantum communication protocol is a quantum key distribution (QKD) scheme that integrates continuous-variable (CV) [6, 7] encoding technology, measurement-device-independent (MDI) [8–10] architecture, and multiparty communication scenarios. It incorporates an untrusted third party to eliminate detector side-channel attacks at all communication nodes, and encodes information using the quadrature components of optical fields to enable the generation of secure shared keys among nodes [7, 11]. Multiparty continuous-variable quantum communication based on GHZ states has been demonstrated in Ref. [12].

When quantum communication transitions from terrestrial fiber-optic communication to space-based satellite communication, a multitude of physical and environmental factors, including gravitation, turbulence, scattering and others, must be taken into consideration. Among these factors, gravitation constitutes a non-negligible and highly influential key element [13–15]. Previous research has shown that curved spacetime exerts an influence on satellite-based quantum communication protocols, equivalent to introducing extra noise into the channel and reducing the coherence between communicating nodes [16, 17].

Gravitational effects are locally equivalent to non-inertial motion, and thus gravity is analogous to the effect of communicating parties' acceleration on quantum states [18]. This equivalence principle has been successfully applied to continuous-variable quantum information protocols [19, 20]. In this framework, each communication node (satellite or ground station) is treated as an idealized rigid accelerating cavity for the localization of quantum field modes (wave packets). This localization enables us to define mode functions adapted to the observer's local reference frame, and the proper acceleration of the cavity is determined by its specific parameters in the gravitational field. Consequently, the communication channel can be described by the Bogoliubov transformation between the mode functions of these individually accelerated cavities, which characterizes the decoherence and noise induced by the curved spacetime background [21]. Previous research efforts have systematically analyzed the impact of non-inertial motion on the information transmission performance of specific cryptographic schemes, focusing on scenarios where single and two communicating parties are in such motion states, respectively [16, 22–24].

This paper aims to extend the analysis of gravitational effects to multiparty quantum communication and construct a multiparty communication scenario in which Alice, Bob and Charlie are all subject to acceleration. We employ symplectic transformations to characterize the evolution of quantum fields across distinct reference frames. The mode functions of inertial frames and non-inertial frames are correlated through Bogoliubov transformations, where the Bogoliubov coefficients are defined by the Klein–Gordon inner product. Finally, through mode mixing and the introduction of thermal noise, the transition of quantum information from inertial to non-inertial frames is realized.

This paper is organized as follows: Section 2 elaborates on the EB scheme for realizing multiparty quantum communication using CV GHZ states, and introduces the basic theoretical framework for the transformation of quantum states from inertial frames to non-inertial frames. Section 3 elaborates on the mechanism by which quantum information transforms from inertial frames to non-inertial frames. Section 4 analyzes the calculation method of the key rate when multiparty quantum communication protocols (QCC, QSS) resist entanglement cloning attacks and coherent attacks under the effect of acceleration. Section 5 analyzes the simulation results. Finally, Section 6 summarizes this research and draws conclusions.

2 | Background

2.1 | Multiparty MDI Quantum Communication Based on GHZ States

Both the entanglement-based (EB) [25] scheme and the prepare-and-measure (PM) [26] scheme are capable of achieving QCC and QSS by employing the MDI approach and CV GHZ states [12]. However, the EB scheme is more amenable to theoretical modeling and security analysis. It can more directly reflect the multiparty CV GHZ correlations, simplify security analysis by means of purification, and be more favorable for handling independent entangled cloning attacks and coherent attacks. Meanwhile, under the covariance matrix framework, the EB scheme also provides a more convenient description of the Gaussian transformations induced by acceleration. Therefore, this section will provide a detailed introduction to the EB scheme illustrated in Figure 1.

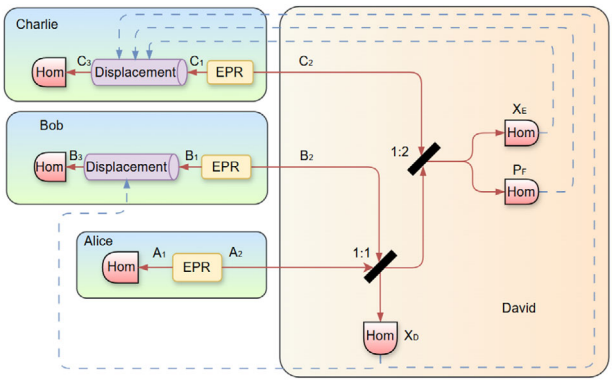

FIGURE 1 | EB scheme.

2.1.1 | Quantum Cryptography Conference

QCC allows each member of a given group to decrypt encrypted messages posted by other members without the members outside the group being able to successfully decrypt them. At its core, key sharing among multiple parties is realized by means of distributed continuous variable GHZ states.

David's Operations: Pass the modes sent by Alice and Bob through a beam splitter with a transmittance of $1/\sqrt{2}$, and perform a homodyne measurement on the position quadrature component $\hat{X}_D$ of the output mode D. Pass the other output mode and the mode sent by Charlie through a beam splitter with a transmittance of $\sqrt{2/3}$, and perform homodyne measurements on the position $\hat{X}_E$ and momentum $\hat{P}_F$ for the output modes E and F, respectively. Publicize the measurement results X_D, X_E, and P_F.

Post-processing: Bob uses $\sqrt{2}X_D$ to perform a displacement operation on the position $\hat{X}_{B1}$ of its retained mode. Charlie uses $\sqrt{1/2}X_D - \sqrt{3/2}X_E$ and $\sqrt{3}P_F$ to perform displacement operations on the position $\hat{X}_{C1}$ and momentum $\hat{P}_{C1}$ of its retained mode, respectively. Eventually, the modes A_1, B_3, and C_3 of Alice, Bob and Charlie form a distributed CV GHZ state, satisfying $\hat{X}_{A1} - \hat{X}_{B3} \to 0$ and $\hat{X}_{B3} - \hat{X}_{C3} \to 0$.

Key Generation: The three parties perform homodyne measurements on the position components, generate a consistent key through data reconciliation and post-selection, and use a one-time pad to achieve secure communication.

2.1.2 | Quantum Secret Sharing

QSS allows members of an authorized group to decrypt a secret through collaboration, while unauthorized groups cannot decrypt it. That is, at least two of the three parties can collaborate to obtain the third party's key.

Same as the EB scheme of QCC, Alice, Bob, and Charlie prepare EPR pairs and send one mode to David.

David's Operations: Same as QCC, publicize the measurement results X_D, X_E, and P_F.

Post-processing: Different from QCC, the three parties perform homodyne measurements on the momentum components. At least two parties share the measurement results, and by using the relationship $\hat{P}_{A1} + \hat{P}_{B3} + \hat{P}_{C3} \to 0$, obtain the third party's key through data reconciliation and post-selection.

2.2 | Gravitational Effect

A real scalar quantum field with mass m satisfies the Klein–Gordon equation $(\Box + m^2)\hat{\Phi} = 0$, in 1 + 1-dimensional Minkowski spacetime taking $c = \hbar = 1$. In Minkowski coordinates, the standard scalar product of this equation is defined as [27]

$$(\phi_1, \phi_2) = i \int_\Sigma \mathrm{d}x \left(\phi_1^\star \partial_t \phi_2 - \phi_2 \partial_t \phi_1^\star\right), \tag{1}$$

where Σ denotes a spacelike Cauchy surface, $(\phi_1, \phi_2) = \left(\phi_2, \phi_1\right)^\star = -\left(\phi_2^\star, \phi_1^\star\right)$.

The field operator $\hat{\Phi}$ can be decomposed into a countable family of modes. (2) represents the decomposition containing positive frequencies with respect to the Minkowski timelike Killing vector field, while (3) denotes the decomposition consisting of positive frequencies with respect to the Rindler timelike Killing vector field.

$$\hat{\Phi} = \sum_k \phi_k \hat{f}_k + \text{H.c.}, \tag{2}$$

$$\hat{\Phi} = \sum_k \psi_k \hat{d}_k + \text{H.c.}, \tag{3}$$

where ϕ_k and ψ_k denote the wave packets associated with the two distinct decomposition modes, whereas $\hat{f}_k$ and $\hat{d}_k$ represent the annihilation operators corresponding to these wave packets.

To enable each party in communication to achieve independent acceleration from one another, localized wave packets ϕ_k in the inertial frame and ψ_k in the non-inertial frame are required, where these wave packets are composed of positive frequencies centered at Ω_0. To render the contribution of negative frequencies negligible, Ω_0 must satisfy $\Omega_0 \gg 1/L$. That is, it is necessary to define the mode functions and their first - order derivatives on the Cauchy surface $t = \eta = 0$ [28, 29]. Thus, in the inertial frame, this chosen mode can be expressed as

$$\begin{aligned} \phi_k(x,0) &= C e^{-2\left(\frac{x_0}{L}\log\frac{x}{x_0}\right)^2} \sin\left(\sqrt{\Omega_0^2 - m^2}(x - x_0)\right), \\ \partial_t \phi_k(x,0) &= -i\Omega_0 \phi_k(x,0), \end{aligned} \tag{4}$$

where x_0 denotes the central position of the mode function, L is the length of its accelerating cavity, and C is a normalization constant. Ω_0 represents the frequency around which the frequency spectrum of the mode function is centered. The parameters L and Ω_0 can be defined independently. Under the condition $|x - x_0| < L$, the approximation $e^{-2\left(\frac{x_0}{L}\log\frac{x}{x_0}\right)^2} \approx e^{-2\left(\frac{x-x_0}{L}\right)^2}$. In Rindler coordinates, i.e., in a non-inertial frame, the mode function at the Cauchy surface $\tau = \eta = 0$ is expressed as [30]

$$\begin{aligned} \psi_k(\chi,0) &= C' e^{-2\left(\frac{x_0}{L}\log\frac{\chi}{x_0}\right)^2} f(\chi), \\ \partial_\tau \psi_k(\chi,0) &= \mp i\Omega_0 \psi_k(\chi,0), \end{aligned} \tag{5}$$

where χ represents the proper distance at the mode center, τ denotes the proper time at the mode center, C' functions as a normalization constant, and $f(\chi)$ is a combination of the modified Bessel functions $I_{i\nu}(x)$ as follows [30]:

$$f(\chi) = \mathrm{Im}\left[I_{-i\frac{\Omega_0}{\mathcal{A}}}(m|x_0|) I_{i\frac{\Omega_0}{\mathcal{A}}}(m|\chi|)\right], \tag{6}$$

where, the zero - frequency truncation is used to eliminate the negative frequencies, and $|x_0| = \frac{1}{\mathcal{A}}$ is additionally chosen to make the spatial positions of the input and output within the local region the same.

In the framework of Gaussian quantum information, the quantum channel acting on the covariance matrix of a Gaussian state can be employed to elucidate the transformation of a quantum state from an inertial reference frame to a non-inertial reference frame. A Gaussian state is fully characterized by two moments. For an n-mode Gaussian state, these moments may be expressed as [31]

$$\begin{aligned} \boldsymbol{X} &= (\langle X_1\rangle, \langle X_2\rangle, \ldots, \langle X_n\rangle), \\ \sigma_{ij} &= \langle X_i X_j + X_j X_i\rangle - 2\langle X_i\rangle\langle X_j\rangle. \end{aligned} \tag{7}$$

Gaussian channels are a subset of quantum channels that map Gaussian states. The input first-order and second-order moments, through the action of the quantum channel $\mathcal{H}(\sigma^{(f)}) = \sigma^{(d)}$ corresponding to Gaussian states, can properly describe the transformation of reference frames, and its specific form is as follows

$$\begin{aligned} X^{(d)} &= MX^{(f)}, \\ \sigma^{(d)} &= M\sigma^{(f)}M^T + N, \end{aligned} \tag{8}$$

where for an n-mode Gaussian channel, M and N are $2n \times 2n$ real matrices. N describes the noise present in the quantum channel and N is a symmetric matrix, i.e., $N = N^T$. f and d correspond to the inertial mode ϕ_k and the accelerated mode ψ_k, respectively.

3 | Acceleration for Multiparty Quantum Communication

To study multiparty quantum communication protocols in a non-inertial scenario, the communicating parties Alice, Bob and Charlie all need to perform independent accelerations. An inertial frame can be transformed into a uniformly accelerating frame using a unitary linear transformation of mode operators [32]. Moreover, since a symplectic transformation is a transformation that preserves the symplectic form and there is a

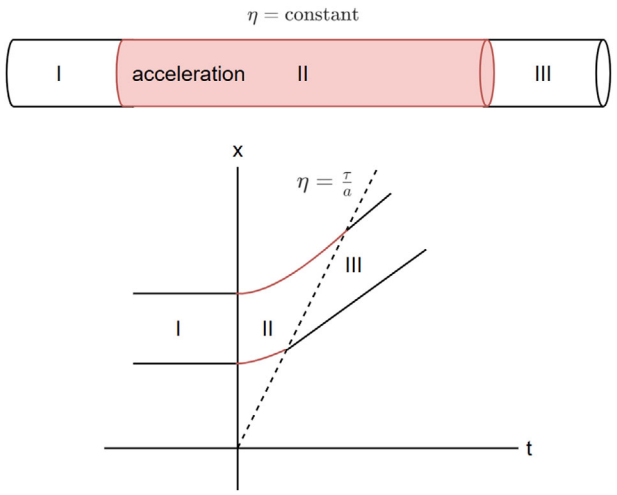

FIGURE 2 | Arbitrary acceleration trajectory. Regions I and III are inertial frames, while region II is an accelerating frame. The acceleration stops at $\eta = \frac{\tau}{a}$.

unique correspondence between a symplectic transformation in phase space and any unitary transformation [33], a symplectic transformation $S_{\mathrm{I,II}}$ can be used to represent the transformation of the quantum field inside the cavity from region I to region II as shown in Figure 2, that is,

$$S\Gamma S^T = \Gamma; \quad \Gamma := \bigoplus_i \Gamma_i, \quad \Gamma_i := \begin{bmatrix} 0 & 1 \\ -1 & 0 \end{bmatrix}. \tag{9}$$

In symplectic transformations, the canonical variables of the bosonic commutation relations are preserved. This property is mathematically expressed by [34]:

$$\left[X_i, X_j\right] = \mathrm{i}\Gamma_{ij}, \tag{10}$$

where the vector of canonical operators is defined as

$$\boldsymbol{X} := (\hat{q}_1, \hat{p}_1, \hat{q}_2, \hat{p}_2, \hat{q}_3, \hat{p}_3) \tag{11}$$

for each mode $i \in \{1, 2, 3\}$, the bosonic position and momentum operators are given by the standard relations:

$$\hat{q}_i := \frac{\hat{a}_i + \hat{a}_i^\dagger}{\sqrt{2}}, \quad \hat{p}_i := \frac{\hat{a}_i - \hat{a}_i^\dagger}{\mathrm{i}\sqrt{2}}, \tag{12}$$

these operators satisfy the canonical commutation relations $[\hat{q}_i, \hat{p}_j] = \mathrm{i}\delta_{ij}$ and $[\hat{q}_i, \hat{q}_j] = [\hat{p}_i, \hat{p}_j] = 0$.

In a cavity with Dirichlet boundary conditions, when the quantum field is expanded using two sets of complete, orthonormal mode functions ϕ_k (in region I, the inertial frame) and ψ_k (in region II, the non-inertial frame) respectively, the Bogoliubov transformation from one reference frame to the other depends on mode overlaps of the following form

$$\hat{d}_k = (\psi_k, \phi_k)\hat{f}_k + (\psi_k, \phi_k^*)\hat{f}_k^\dagger, \tag{13}$$

where $k \in \{1, 2, 3\}$.

The mode functions and ladder operators via the Bogoliubov transformation are as follows:

$$\psi_j = \sum_i \tilde{\alpha}_{ij}\phi_i + \tilde{\beta}_{ij}\phi_i^*, \tag{14}$$

$$\hat{b}_j = \sum_i \tilde{\alpha}_{ij}^*\hat{a}_i - \tilde{\beta}_{ij}^*\hat{a}_i^\dagger, \tag{15}$$

where $\tilde{\alpha}_{ij} := (\psi_i, \phi_j)$ and $\tilde{\beta}_{ij} := -(\psi_i, \phi_j^*)$ are Bogoliubov coefficients. i and j represent the number of modes, which take values of 1, 2 and 3 in this scheme, meaning three modes correspond to three communicators. $(\cdot, \cdot)$ denotes the Klein–Gordon inner product [35].

The transformation from the accelerating frame in region II back to the inertial frame is the inverse transformation of S_{II}, that is, $S_{\mathrm{II,III}} = S_{\mathrm{II}}^{-1}$. Moreover, since in the free evolution within region II, $S_{\mathrm{II}} = \bigoplus_j G_j$, where G_j is a kind of rotational transformation in phase space, the full symplectic transformation representing the evolution of the field from region I to region III (i.e., from the inertial frame to the accelerating frame and then back to the inertial frame as illustrated in Figure 3) can be expressed as

$$S = S_{\mathrm{I,II}}^{-1} S_{\mathrm{II}} S_{\mathrm{I,II}} = \begin{bmatrix} M_{11} & M_{12} & M_{13} \\ M_{21} & M_{22} & M_{23} \\ M_{31} & M_{32} & M_{33} \end{bmatrix}, \tag{16}$$

where

$$M_{ij} = \begin{bmatrix} \mathrm{Re}(\alpha_{ij} - \beta_{ij}) & \mathrm{Im}(\alpha_{ij} + \beta_{ij}) \\ -\mathrm{Im}(\alpha_{ij} - \beta_{ij}) & \mathrm{Re}(\alpha_{ij} + \beta_{ij}) \end{bmatrix}, \tag{17}$$

the Bogoliubov coefficients α_{ij} and β_{ij} can be defined as:

$$\begin{aligned} \alpha_{ij} &= (\psi_i, \phi_j), \\ \beta_{ij} &= -(\psi_i, \phi_j^*). \end{aligned} \tag{18}$$

The Bogoliubov coefficients can be series-expanded with respect to the dimensionless parameter h through perturbation, and the specific form is given below [31]:

$$\begin{aligned} \alpha_{ij} &= \alpha_{ij}^{(0)} + \alpha_{ij}^{(1)}h + \alpha_{ij}^{(2)}h^2 + O(h^3), \\ \beta_{ij} &= \beta_{ij}^{(0)} + \beta_{ij}^{(1)}h + \beta_{ij}^{(2)}h^2 + O(h^3), \end{aligned} \tag{19}$$

where the dimensionless parameter h is defined as $h = aL$, where a is related to the acceleration and L denotes the length of the cavity.

From the Bogoliubov identity, it can be derived that [31]

$$\sum_i |\alpha_{ij}|^2 - |\beta_{ij}|^2 = 1. \tag{20}$$

In the perturbation coefficients of the Bogoliubov expansion in terms of the dimensionless parameter [36], if $(i + j)$ is an even number, then $\alpha_{ij}^{(1)} = \beta_{ij}^{(1)} = 0$. For the zeroth-order and second-order terms of Equation (20), using the perturbation series expansion of the Bogoliubov coefficients in Equation (19), it can

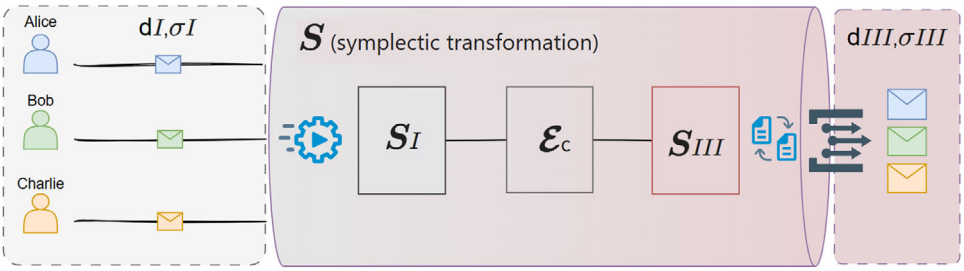

FIGURE 3 | The evolution of information in a Gaussian channel under the influence of multiparty quantum communication acceleration. Alice, Bob, and Charlie utilize the cavity's first mode for quantum information encoding and decoding. After applying a symplectic transformation S, the remaining modes are neglected. The standard Gaussian channel $\mathcal{E}$ is decomposed into canonical form $\mathcal{E}_c$ through two symplectic transformations S_{I} and S_{III} in regions I and III.

be obtained that

$$\left|\alpha_{ij}^{(0)}\right|^2 = 1, \tag{21}$$

$$\mathrm{Re}\left(\alpha_{jj}^{(0)*}\alpha_{jj}^{(2)}\right) + f_{\alpha,k} - f_{\beta,k} = 0, \tag{22}$$

where

$$f_{\alpha,k} := \frac{1}{2}\sum_{n\neq k}\left|\alpha_{nk}^{(1)}\right|^2,$$
$$f_{\beta,k} := \frac{1}{2}\sum_{n\neq k}\left|\beta_{nk}^{(1)}\right|^2. \tag{23}$$

Based on Equation (21) and combined with the unitarity of quantum field mode transformations, it can be derived that:

$$\alpha_{ij}^{(0)} = \delta_{ij}e^{i\phi_j}, \tag{24}$$

where ϕ_j is defined as $2\pi ju$, it represents the phase acquired by mode j relative to the cavity's center position when the cavity undergoes accelerating motion over the proper time τ and u is defined as $\frac{h\tau}{4\mathrm{Larctanh}(h/2)}$. In e^i, i denotes the imaginary unit [32].

The first-order coefficients of the perturbation expansion can be obtained by relating the solutions of the Klein–Gordon equation in the inertial frame and the accelerated frame, with the specific form given as follows [37, 38]:

$$\alpha_{ij}^{(1)} = \frac{-2\sqrt{ij}}{\pi^2(j-i)^3}\beta_{ij}^{(1)} = \frac{2\sqrt{ij}}{\pi^2(i+j)^3}, \tag{25}$$

where the sum $i + j$ is not an even number.

In this study, among all the modes decomposed in the Minkowski frame, except for the mode ϕ_k, all other modes and their corresponding annihilation operators $\hat{f}_{\mathrm{k}}$ are in the vacuum state. In all the modes decomposed in the Rindler frame, although the modes $\psi_{k\neq\{\mathrm{k}\}}$ (other than the mode ψ_k and its corresponding annihilation operator $\hat{d}_{\mathrm{k}}$) are non - vacuum modes, they are chosen to be neglected. Therefore, in three - mode multiparty quantum communication, assuming that the mode functions ϕ_{I}, ψ_{I}, ϕ_{II}, ψ_{II}, ϕ_{III}, and ψ_{III} do not overlap with one another, it can be obtained that:

$$(\phi_{\mathrm{I}}, \phi_{\mathrm{II}}^{(*)}) = (\psi_{\mathrm{I}}, \psi_{\mathrm{II}}^{(*)}) = (\phi_{\mathrm{I}}, \psi_{\mathrm{II}}^{(*)}) = (\phi_{\mathrm{II}}, \psi_{\mathrm{I}}^{(*)}) = 0,$$
$$(\phi_{\mathrm{I}}, \phi_{\mathrm{III}}^{(*)}) = (\psi_{\mathrm{I}}, \psi_{\mathrm{III}}^{(*)}) = (\phi_{\mathrm{I}}, \psi_{\mathrm{III}}^{(*)}) = (\phi_{\mathrm{III}}, \psi_{\mathrm{I}}^{(*)}) = 0,$$
$$(\phi_{\mathrm{II}}, \phi_{\mathrm{III}}^{(*)}) = (\psi_{\mathrm{II}}, \psi_{\mathrm{III}}^{(*)}) = (\phi_{\mathrm{II}}, \psi_{\mathrm{III}}^{(*)}) = (\phi_{\mathrm{III}}, \psi_{\mathrm{II}}^{(*)}) = 0, \tag{26}$$

and

$$[\hat{f}_{\mathrm{I}}, \hat{f}_{\mathrm{II}}^{(\dagger)}] = [\hat{d}_{\mathrm{I}}, \hat{d}_{\mathrm{II}}^{(\dagger)}] = [\hat{f}_{\mathrm{I}}, \hat{d}_{\mathrm{II}}^{(\dagger)}] = [\hat{f}_{\mathrm{II}}, \hat{d}_{\mathrm{I}}^{(\dagger)}] = 0,$$
$$[\hat{f}_{\mathrm{I}}, \hat{f}_{\mathrm{III}}^{(\dagger)}] = [\hat{d}_{\mathrm{I}}, \hat{d}_{\mathrm{III}}^{(\dagger)}] = [\hat{f}_{\mathrm{I}}, \hat{d}_{\mathrm{III}}^{(\dagger)}] = [\hat{f}_{\mathrm{III}}, \hat{d}_{\mathrm{I}}^{(\dagger)}] = 0,$$
$$[\hat{f}_{\mathrm{II}}, \hat{f}_{\mathrm{III}}^{(\dagger)}] = [\hat{d}_{\mathrm{II}}, \hat{d}_{\mathrm{III}}^{(\dagger)}] = [\hat{f}_{\mathrm{II}}, \hat{d}_{\mathrm{III}}^{(\dagger)}] = [\hat{f}_{\mathrm{III}}, \hat{d}_{\mathrm{II}}^{(\dagger)}] = 0, \tag{27}$$

where the symbol $^{(*)}$ indicates that the equality holds regardless of the presence or absence of complex conjugation.

Thus, except for the mode k of the Gaussian state, all other modes are removed. Then, the matrices M and Ncorresponding to mode k can be expressed as [31]

$$M_{kk} = \begin{bmatrix} \mathrm{Re}(\alpha_{kk} - \beta_{kk}) & \mathrm{Im}(\alpha_{kk} + \beta_{kk}) \\ -\mathrm{Im}(\alpha_{kk} - \beta_{kk}) & \mathrm{Re}(\alpha_{kk} + \beta_{kk}) \end{bmatrix}, \tag{28}$$

$$N_k = \sum_{n\neq k} M_{nk}M_{nk}^T \tag{29}$$

when the above equations are expanded perturbatively in terms of the dimensionless parameter $h = aL$ and third- and higher-order contributions are neglected, it follows that [31]

$$M_{kk} = M_{\phi_a}^{(0)} + M_{kk}^{(2)}h^2 + O(h^3),$$
$$N_k = N_k^{(2)}h^2 + O(h^3),$$
$$N_k^{(2)} = \sum_{n\neq k} M_{nk}^{(1)}\left(M_{nk}^{(1)}\right)^T,$$
$$M_{\phi_a}^{(0)} = \begin{bmatrix} \cos\phi_a & \sin\phi_a \\ -\sin\phi_a & \cos\phi_a \end{bmatrix},$$
$$M_{nk}^{(0)} = M_{kk}^{(1)} = 0\,(n \neq k),$$
$$M_{nk}^{(m)} = \begin{bmatrix} \mathrm{Re}\left(\alpha_{nk}^{(m)} - \beta_{nk}^{(m)}\right) & \mathrm{Im}\left(\alpha_{nk}^{(m)} + \beta_{nk}^{(m)}\right) \\ -\mathrm{Im}\left(\alpha_{nk}^{(m)} - \beta_{nk}^{(m)}\right) & \mathrm{Re}\left(\alpha_{nk}^{(m)} + \beta_{nk}^{(m)}\right) \end{bmatrix}, \tag{30}$$

where in the last matrix $m = 1, 2$ because the third-order effect is neglected.

When a Gaussian state undergoes free evolution while moving inertially in a Gaussian channel within the proper time τ_i, the zeroth - order matrix of M can be expressed as

$$M_{\phi_i}^{(0)} = \begin{bmatrix} \cos\phi_i & -\sin\phi_i \\ \sin\phi_i & \cos\phi_i \end{bmatrix}, \tag{31}$$

where $\phi_i = \frac{k\pi\tau_i}{L_i}$ denotes the phase accumulated during the free evolution of the cavity within the fixed time τ_i, where k is the corresponding mode with $k \in \{1, 2, 3\}$ and $i \in \{1, 2, 3\}$. To simplify the calculation, it is assumed that the phase shift satisfies $\phi_i = \pi - 2\phi_a$.

Then, the acceleration matrix satisfying multiparty quantum synchronization is constructed as

$$M = \begin{bmatrix} \mathrm{Re}(\alpha_{11}-\beta_{11}) & \mathrm{Im}(\alpha_{11}+\beta_{11}) & 0 & 0 & 0 & 0 \\ -\mathrm{Im}(\alpha_{11}-\beta_{11}) & \mathrm{Re}(\alpha_{11}+\beta_{11}) & 0 & 0 & 0 & 0 \\ 0 & 0 & \mathrm{Re}(\alpha_{22}-\beta_{22}) & \mathrm{Im}(\alpha_{22}+\beta_{22}) & 0 & 0 \\ 0 & 0 & -\mathrm{Im}(\alpha_{22}-\beta_{22}) & \mathrm{Re}(\alpha_{22}+\beta_{22}) & 0 & 0 \\ 0 & 0 & 0 & 0 & \mathrm{Re}(\alpha_{33}-\beta_{33}) & \mathrm{Im}(\alpha_{33}+\beta_{33}) \\ 0 & 0 & 0 & 0 & -\mathrm{Im}(\alpha_{33}-\beta_{33}) & \mathrm{Re}(\alpha_{33}+\beta_{33}) \end{bmatrix}. \tag{32}$$

In cases where noise in the cavity of a Gaussian channel cannot be neglected, the influence of acceleration on multiparty quantum communication can be expressed as

$$\begin{aligned} \sigma^{(d)} &= \boldsymbol{M}\boldsymbol{\sigma}^{(f)}\boldsymbol{M}^{\mathrm{T}} + \boldsymbol{N} \\ &= \begin{bmatrix} \boldsymbol{M}_{11}\boldsymbol{\sigma}_{11}^{(f)}\boldsymbol{M}_{11}^{\mathrm{T}} + \boldsymbol{N}_I & \boldsymbol{M}_{11}\boldsymbol{\sigma}_{12}^{(f)}\boldsymbol{M}_{22}^{\mathrm{T}} & \boldsymbol{M}_{11}\boldsymbol{\sigma}_{13}^{(f)}\boldsymbol{M}_{33}^{\mathrm{T}} \\ \boldsymbol{M}_{22}\boldsymbol{\sigma}_{21}^{(f)}\boldsymbol{M}_{11}^{\mathrm{T}} & \boldsymbol{M}_{22}\boldsymbol{\sigma}_{22}^{(f)}\boldsymbol{M}_{22}^{\mathrm{T}} + \boldsymbol{N}_{II} & \boldsymbol{M}_{22}\boldsymbol{\sigma}_{23}^{(f)}\boldsymbol{M}_{33}^{\mathrm{T}} \\ \boldsymbol{M}_{33}\boldsymbol{\sigma}_{31}^{(f)}\boldsymbol{M}_{11}^{\mathrm{T}} & \boldsymbol{M}_{33}\boldsymbol{\sigma}_{32}^{(f)}\boldsymbol{M}_{22}^{\mathrm{T}} & \boldsymbol{M}_{33}\boldsymbol{\sigma}_{33}^{(f)}\boldsymbol{M}_{33}^{\mathrm{T}} + \boldsymbol{N}_{III} \end{bmatrix}, \end{aligned} \tag{33}$$

where the block matrix $\boldsymbol{\sigma}^{(f)} = \begin{bmatrix} \boldsymbol{\sigma}_{(11)}^{(f)} & \boldsymbol{\sigma}_{(12)}^{(f)} & \boldsymbol{\sigma}_{(13)}^{(f)} \\ \boldsymbol{\sigma}_{(21)}^{(f)} & \boldsymbol{\sigma}_{(22)}^{(f)} & \boldsymbol{\sigma}_{(23)}^{(f)} \\ \boldsymbol{\sigma}_{(31)}^{(f)} & \boldsymbol{\sigma}_{(32)}^{(f)} & \boldsymbol{\sigma}_{(33)}^{(f)} \end{bmatrix}$, N_I, N_{II} and N_{III} are defined as follows

$$\begin{aligned} \boldsymbol{N}_I &= h^2 \begin{bmatrix} \gamma_{1_{A_{21}}}^2 + \gamma_{2_{A_{21}}}^2 + \gamma_{1_{A_{31}}}^2 + \gamma_{2_{A_{31}}}^2 & \gamma_{1_{A_{21}}}\gamma_{3_{A_{21}}} + \gamma_{2_{A_{21}}}\gamma_{4_{A_{21}}} + \gamma_{1_{A_{31}}}\gamma_{3_{A_{31}}} + \gamma_{2_{A_{31}}}\gamma_{4_{A_{31}}} \\ \gamma_{3_{A_{21}}}\gamma_{1_{A_{21}}} + \gamma_{4_{A_{21}}}\gamma_{2_{A_{21}}} + \gamma_{3_{A_{31}}}\gamma_{1_{A_{31}}} + \gamma_{4_{A_{31}}}\gamma_{2_{A_{31}}} & \gamma_{3_{A_{21}}}^2 + \gamma_{4_{A_{21}}}^2 + \gamma_{3_{A_{31}}}^2 + \gamma_{4_{A_{31}}}^2 \end{bmatrix}, \\ \boldsymbol{N}_{II} &= h^2 \begin{bmatrix} \gamma_{1_{B_{12}}}^2 + \gamma_{2_{B_{12}}}^2 + \gamma_{1_{B_{32}}}^2 + \gamma_{2_{B_{32}}}^2 & \gamma_{1_{B_{12}}}\gamma_{3_{B_{12}}} + \gamma_{2_{B_{12}}}\gamma_{4_{B_{12}}} + \gamma_{1_{B_{32}}}\gamma_{3_{B_{32}}} + \gamma_{2_{B_{32}}}\gamma_{4_{B_{32}}} \\ \gamma_{3_{B_{12}}}\gamma_{1_{B_{12}}} + \gamma_{4_{B_{12}}}\gamma_{2_{B_{12}}} + \gamma_{3_{B_{32}}}\gamma_{1_{B_{32}}} + \gamma_{4_{B_{32}}}\gamma_{2_{B_{32}}} & \gamma_{3_{B_{12}}}^2 + \gamma_{4_{B_{12}}}^2 + \gamma_{3_{B_{32}}}^2 + \gamma_{4_{B_{32}}}^2 \end{bmatrix}, \\ \boldsymbol{N}_{III} &= h^2 \begin{bmatrix} \gamma_{1_{C_{13}}}^2 + \gamma_{2_{C_{13}}}^2 + \gamma_{1_{C_{23}}}^2 + \gamma_{2_{C_{23}}}^2 & \gamma_{1_{C_{13}}}\gamma_{3_{C_{13}}} + \gamma_{2_{C_{13}}}\gamma_{4_{C_{13}}} + \gamma_{1_{C_{23}}}\gamma_{3_{C_{23}}} + \gamma_{2_{C_{23}}}\gamma_{4_{C_{23}}} \\ \gamma_{3_{C_{13}}}\gamma_{1_{C_{13}}} + \gamma_{4_{C_{13}}}\gamma_{2_{C_{13}}} + \gamma_{3_{C_{23}}}\gamma_{1_{C_{23}}} + \gamma_{4_{C_{23}}}\gamma_{2_{C_{23}}} & \gamma_{3_{C_{13}}}^2 + \gamma_{4_{C_{13}}}^2 + \gamma_{3_{C_{23}}}^2 + \gamma_{4_{C_{23}}}^2 \end{bmatrix}, \end{aligned} \tag{34}$$

the components of the parameter γ are defined as: $\begin{cases} \gamma_{1_{V_{ij}}} = \mathrm{Re}(\alpha_{ij} - \beta_{ij}) \\ \gamma_{2_{V_{ij}}} = \mathrm{Im}(\alpha_{ij} + \beta_{ij}) \\ \gamma_{3_{V_{ij}}} = -\mathrm{Im}(\alpha_{ij} - \beta_{ij}) \\ \gamma_{4_{V_{ij}}} = \mathrm{Re}(\alpha_{ij} + \beta_{ij}) \end{cases}$, where $V \in \{A, B, C\}$ corresponds to Mode I, II, and III, respectively. The sub - matrices $\boldsymbol{\sigma}_{(ij)}^{(f)}$ within $\boldsymbol{\sigma}^{(f)}$ are defined as 2×2 matrices: $\boldsymbol{\sigma}_{ij}^{(f)} = \begin{bmatrix} a_{ij} & b_{ij} \\ c_{ij} & d_{ij} \end{bmatrix}$. Matrices $\boldsymbol{M}$ and the parameter h have been discussed previously and will not be repeated here.

4 | Key Rate Calculation

Next, we will explore the impact of acceleration on the security of multiparty QCC and QSS.

4.1 | Independent Entangled Cloning Attack

In this subsection, we analyze the independent entangled cloning attack in the presence of acceleration. As shown in Figure 4, initially, the eavesdropper Eve prepares three sets of independent EPR pairs. Under the acceleration effect, Eve injects one mode of each EPR pair into the channel through a beam splitter with transmittance η_A (and η_B, η_C for the other pairs). After passing through the beam splitter, the output mode is $\hat{E}_{A1(B1,C1)}$, while the other output mode of the EPR pair is $\hat{E}_{A2(B2,C2)}$. These two output modes are stored in separate quantum memories (QMs), respectively. Through the transformation in Formula Equation (33) applied to the multiparty quantum communication matrix $\mathbf{V}_{A1,B3,C3,\mathrm{Eve}}$ [12], the covariance matrix $\mathbf{W}$ of the state $\rho_{A1,B3,C3,\mathrm{Eve}}$ under the influence of acceleration can be obtained.

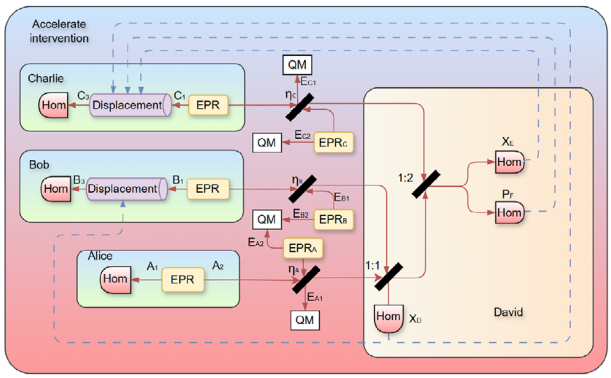

FIGURE 4 | The EB scheme against an independent entangled cloning attack in the presence of acceleration.

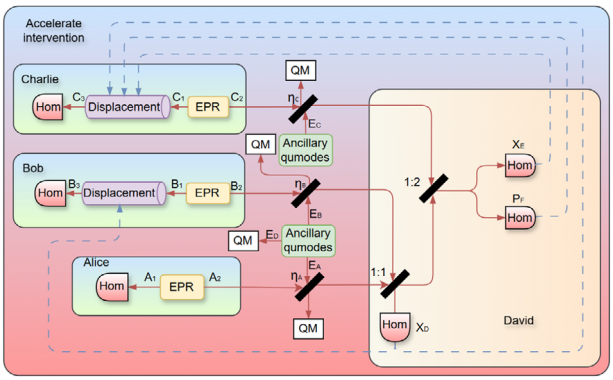

FIGURE 5 | The EB scheme against coherent attack under the influence of acceleration.

In the QCC, assuming that Alice shares her secret message with Bob and Charlie, the key rate can be defined as

$$K_{\mathrm{QCC}}^{(d)} = \min\{K_{AB}^{(d)}, K_{AC}^{(d)}\}, \tag{35}$$

the key rates for reverse reconciliation and direct reconciliation, are given by Equations (36) and (37), respectively.

$$\begin{aligned} K_{AB}^{\mathrm{RR}(d)} &= \beta I(A_m : B_n) - I(A_m : E_s) \\ K_{AC}^{\mathrm{RR}(d)} &= \beta I(A_m : C_n) - I(A_m : E_s) \end{aligned} \tag{36}$$

$$\begin{aligned} K_{AB}^{\mathrm{DR}(d)} &= \beta I(A_m : B_n) - I(B_n : E_s) \\ K_{AC}^{\mathrm{DR}(d)} &= \beta I(A_m : C_n) - I(C_n : E_s) \end{aligned} \tag{37}$$

where K_{AB} denotes the key rate between Alice and Bob, K_{AC} denotes the key rate between Alice and Charlie, and β is the reconciliation efficiency. $I(A_m : B_n)$, $I(A_m : C_n)$, $I(A_m : E_s)$, $I(B_n : E_s)$ and $I(C_n : E_s)$ denote the mutual information between the measured data of Alice and Bob, Alice and Charlie, Alice and Eve, Bob and Eve, and Charlie and Eve, respectively.

The mutual information between the measured data of Alice and Bob, and between Alice and Charlie, can be calculated using Equation (38), while the mutual information of other measured data pairs is obtained via Equation (39).

$$I(A_m : B_n(C_n)) = \frac{1}{2}\log_2 \frac{\mathbf{W}(\hat{B_n}(\hat{C_n}))}{\mathbf{W}(\hat{B_n}(\hat{C_n}))|A_m)} \tag{38}$$

$$I(A_m(B_n, C_n) : E_s) = \frac{1}{2}\log_2 \frac{\mathbf{W}(\hat{A_m}(\hat{B_n}, \hat{C_n})}{\mathbf{W}(\hat{A_m}(\hat{B_n}, \hat{C_n})|E_s)}, \tag{39}$$

where $\mathbf{W}(\hat{B}_n(\hat{C}_n)) \mid A_m)$ denotes the conditional variance of $\hat{B}_n$ and $\hat{C}_n$ after the homodyne detection of $\hat{A}_m$, and $\mathbf{W}(\hat{A}_m(\hat{B}_n, \hat{C}_n)) \mid E_s)$ represents the conditional variance of $\hat{A}_m$, $\hat{B}_n$, and $\hat{C}_n$ following the homodyne detection of $\hat{E}_s$.

In QSS, assuming that Charlie holds the key, the key rates for reverse reconciliation and direct reconciliation are given by Equations (40) and (41) respectively.

$$K_{\mathrm{QSS}}^{\mathrm{RR}(d)} = \beta I(A_m, B_n : C_n) - I(C_n : E_s), \tag{40}$$

$$K_{\mathrm{QSS}}^{\mathrm{DR}(d)} = \beta I(A_m, B_n : C_n) - I(A_m : E_s) - I(B_n : E_s). \tag{41}$$

The mutual information of the measurement data can be expressed as Equations (42), (43) and (44), respectively.

$$I(A_m, B_n : C_n) = \frac{1}{2}\log_2 \frac{\mathbf{W}(\hat{C_n})}{\mathbf{W}(\hat{C_n} \mid A_m, B_n)} \tag{42}$$

$$I(C_n : E_s) = \frac{1}{2}\log_2 \frac{\mathbf{W}(\hat{C_n})}{\mathbf{W}(\hat{C_n} \mid E_s)} \tag{43}$$

$$I(A_m : E_s) + I(B_n : E_s) = \frac{1}{2}\log_2 \frac{\mathbf{W}(\hat{A_m})}{\mathbf{W}(\hat{A_m}|E_s)} + \frac{1}{2}\log_2 \frac{\mathbf{W}(\hat{B_n})}{\mathbf{W}(\hat{B_n}|E_s)}. \tag{44}$$

In the above equations, the parameters are $m = 1$ and $n = 3$. Specifically, for the mutual information $I(A_m : E_s)$between Alice's and Eve's measured data, $s = \{A_1, A_2\}$; for the mutual information $I(B_n : E_s)$between Bob's and Eve's measured data, $s = \{B_1, B_2\}$; and for the mutual information $I(C_n : E_s)$ between Charlie's and Eve's measured data, $s = \{C_1, C_2\}$.

4.2 | Coherent Attack

In this section, we will investigate the coherent attack under the acceleration effect. As shown in Figure 5, in the auxiliary quantum mode, Eve extracts three quantum modes and injects them into three channels through beam splitters with transmittance $\eta_{A(B,C)}$ respectively; both the output states of the beam splitters and the retained auxiliary quantum modes after output are stored in Eve's QM. The multiparty quantum communication matrix $\mathbf{V}_{A1,B3,C3|X_D,X_E,\hat{P}_F}$ in the non-inertial frame can be expressed as [12]

$$\mathbf{V}_{A1,B3,C3|X_D,X_E,\hat{P}_F} = \begin{bmatrix} A & 0 & B & 0 & B & 0 \\ 0 & C & 0 & D & 0 & D \\ B & 0 & E & 0 & F & 0 \\ 0 & D & 0 & G & 0 & H \\ B & 0 & F & 0 & E & 0 \\ 0 & D & 0 & H & 0 & G \end{bmatrix} \tag{45}$$

Where parameters A, B, C, D, E, F, G, and H are too complex to present here and are thus provided in Appendix.

By performing the operation in Equation (33) using this covariance matrix, the covariance matrix $\mathbf{W}$ under the influence of acceleration can be obtained. After acquiring the covariance matrix under the influence of acceleration, the key rate of the QCC scheme can be expressed as

$$\begin{aligned} K_{\mathrm{AB}}^{\mathrm{RR}(d)} &= \beta I(A_m : B_n) - H(\rho_{\mathrm{Eve}} : A_m), \\ K_{\mathrm{AC}}^{\mathrm{RR}(d)} &= \beta I(A_m : C_n) - H(\rho_{\mathrm{Eve}} : A_m), \end{aligned} \tag{46}$$

where $I(A_m : B_n(C_n))$ is the mutual information, and $H(\rho_{\mathrm{Eve}} : A_m)$ is the Holevo quantity between Eve and the quantum state ρ of the measurement data A_m, which can be expressed as

$$H(\rho_{\mathrm{Eve}} : A_m) = S(\rho_{A_m,B_n,C_n}) - S(\rho_{B_n,C_n|A_m}) \tag{47}$$

where $S(\rho)$ denotes the von Neumann entropy of the quantum state ρ.

Using the symplectic eigenvalues ν_1, ν_2, ν_3 of the covariance matrix $\mathbf{W}_{A_m,B_n,C_n}$ and the symplectic eigenvalues ν_4 and ν_5 of the conditional covariance matrix $\mathbf{W}_{B_n,C_n|A_m}$, one can compute the entropy $S(\rho_{A_m,B_n,C_n})$of the state ρ_{A_m,B_n,C_n} and the conditional entropy $S(\rho_{B_n,C_n|A_m})$:

$$S(\rho_{A_m,B_n,C_n}) = h(\nu_1) + h(\nu_2) + h(\nu_3), \tag{48}$$

$$S(\rho_{B_n,C_n|A_m}) = h(\nu_4) + h(\nu_5), \tag{49}$$

where

$$h(x) := \frac{x+1}{2}\log_2\frac{x+1}{2} - \frac{x-1}{2}\log_2\frac{x-1}{2}. \tag{50}$$

The key rate of the QSS scheme is given by

$$K_{\mathrm{QSS}}^{\mathrm{RR}(d)} = \beta\, I\left(A_m, B_n : C_n\right) - H\left(\rho_{\mathrm{Eve}} : C_n\right) \tag{51}$$

where

$$\begin{aligned} H\left(\rho_{\mathrm{Eve}} : C_n\right) &= S\left(\rho_{\mathrm{Eve}}\right) - S\left(\rho_{\mathrm{Eve}|C_n}\right) \\ &= S\left(\rho_{A_m,B_n,C_n}\right) - S\left(\rho_{A_m,B_n|C_n}\right). \end{aligned} \tag{52}$$

Using the symplectic eigenvalues ν_6 and ν_7 of the covariance matrix $\mathbf{W}_{A_m,B_n|C_n}$, one can compute the conditional entropy $S(\rho_{A_m,B_n|C_n})$:

$$S(\rho_{A_m,B_n|C_n}) = h(\nu_6) + h(\nu_7). \tag{53}$$

It is worth noting that the key recovery situation for QSS with (3,4) and even higher thresholds may be different [39, 40].

5 | Simulation

In this section, we will analyze the impact of acceleration on the simulation results of QCC and QSS under coherent attacks, where the three communicating parties (Alice, Bob and Charlie) have equal weights in the communication process.

Settings of relevant parameters. The channel transmittance between Alice, Bob, Charlie and David is denoted as $\eta_{A(B,C)} = 10^{-\frac{L_{A(B,C)}}{10}}$, where $L_{A(B,C)}$ represents the transmission distance between the three communicating parties and David. In addition, $\mathcal{A}$ stands for the acceleration generated during the communication process. V is the variance of the two-mode squeezed state (TMSS) adopted by Alice, Bob, and Charlie. V_{E_A}, V_{E_B}, and V_{E_C} respectively represent the thermal noise injected by Eve into the corresponding channels. g_1, g_2, and g_3 denote the correlation between channel noises. β indicates the reconciliation efficiency, which is set to 0.98 in the simulation.

5.1 | Quantum Cryptography Conference

This section investigates the impact of different accelerations on the secure communication key in QCC under the scenario where Eve launches a symmetric attack on Bob and Charlie.

Since the channels of Bob and Charlie are subjected to the same symmetric attack by Eve, $V_{E_B} = V_{E_C}$ and $g_1 = g_2$. Meanwhile, assume that the transmission distance from Alice to David is set differently from that between Bob and Charlie to David, while the transmission distance between Bob and Charlie to David is identical. i.e., $L_A \neq L_B = L_C$.

Figure 6 illustrates the variation of the maximum transmission distance between communicating parties when $K_{QCC}^{\mathrm{RR}} > 0$ under the influence of different accelerations. As expected, acceleration undermines the maximum transmission distance between communicating parties, regardless of whether the attack employed is one of the two types of maximum entanglement attacks or an independent attack.

Figure 8 illustrates the impact of acceleration on the secure key and transmission distance under entanglement attacks and independent attacks when $\mathcal{A} = 0.1$, as well as their variation trends. It can be seen that acceleration degrades both the secure key rate and the maximum transmission distance under all attack models, with the degradation being more pronounced for independent attacks than for entanglement attacks.

Figure 7 illustrates the variation of the key rate with different distances between Bob(Charlie) and David, the influence of varying thermal noises injected by Eve, and the effect of the variance V of the initial TMSS adopted by Alice (Bob, Charlie). These results are obtained under the entanglement attack scenario where $g_1 = 0$, and $g_3 = -\sqrt{V_{E_C}^2 - 1}$. It can be observed that the key rate decreases gradually as $L_B = L_C$ increases, and the stronger the thermal noise injected by Eve, the more rapid the key rate decline. However, an increase in the variance V of the initial TMSS results in a higher key rate. Notably, the variation trends are similar in both the inertial frame and the non-inertial frame, with acceleration only further impairing the key rate.

Figure 9 illustrates the three-dimensional relationship among acceleration, key rate, and channel loss under maximum

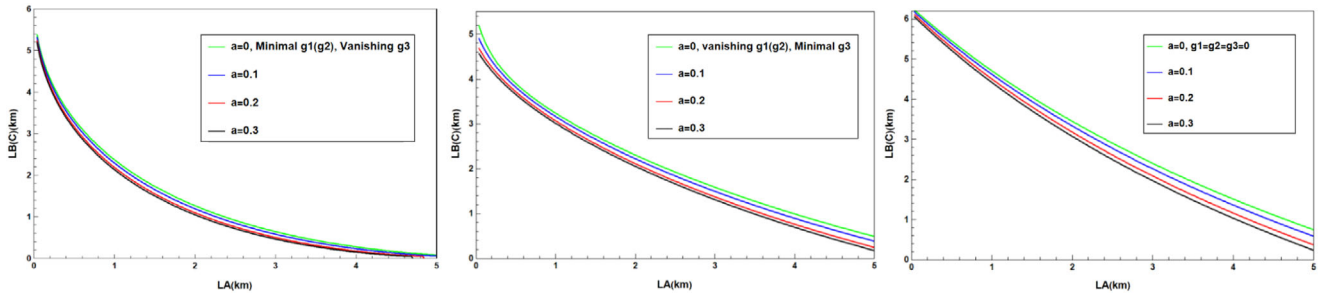

FIGURE 6 | Variation of maximum communication distance with acceleration under different maximum entanglement attacks and independent attacks when $K_{\mathrm{QCC}}^{\mathrm{RR}} > 0$. The green curve corresponds to $\mathcal{A} = 0$, the blue curve to $\mathcal{A} = 0.1$, the red curve to $\mathcal{A} = 0.2$, and the black curve to $\mathcal{A} = 0.3$. The left subplot depicts the maximum entanglement attack scenario where $g_1 = -\sqrt{3/2}$ and $g_3 = 0$. The middle subplot corresponds to the maximum entanglement attack scenario where $g_1 = 0$ and $g_3 = -\sqrt{3}$. The right subplot represents the independent attack scenario with $g_1 = g_3 = 0$. Other parameter settings: $V = 20$, $V_{E_A} = V_{E_B} = V_{E_C} = 2$, $\eta_{A(B,C)} = 10^{-\frac{L_{A(B,C)}}{10}}$.

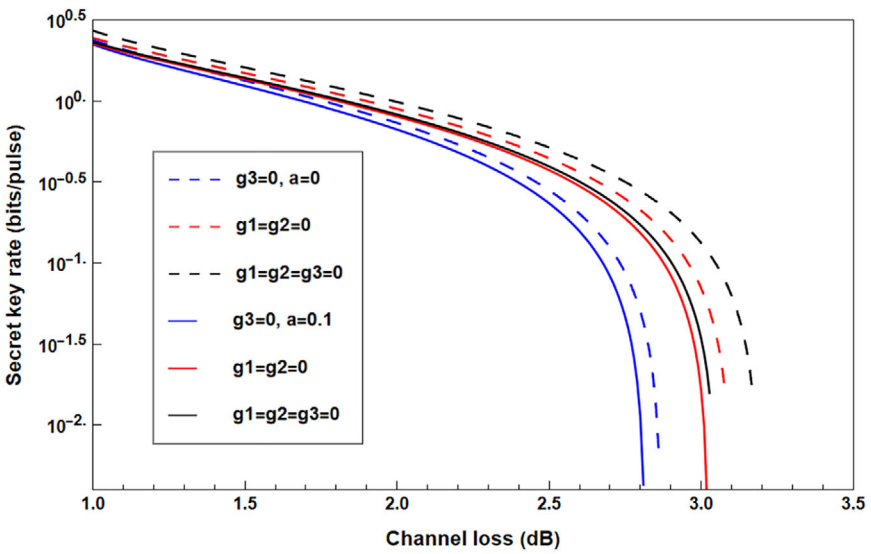

FIGURE 7 | Impact of acceleration on the key rate. The dashed line corresponds to $\mathcal{A} = 0$, and the solid line corresponds to $\mathcal{A} = 0.1$. The blue line denotes the entanglement scenario where $g_1 = -\sqrt{(V_{E_C}^2 - 1)/2}$ and $g_3 = 0$; the red line represents the entanglement scenario where $g_1 = 0$ and $g_3 = -\sqrt{V_{E_C}^2 - 1}$; the black line indicates the independent attack scenario with $g_1 = g_3 = 0$. Other parameter settings: $V = 30$, $V_{E_A} = V_{E_B} = V_{E_C} = 1.03$, and $L_B = L_C = 0.1$.

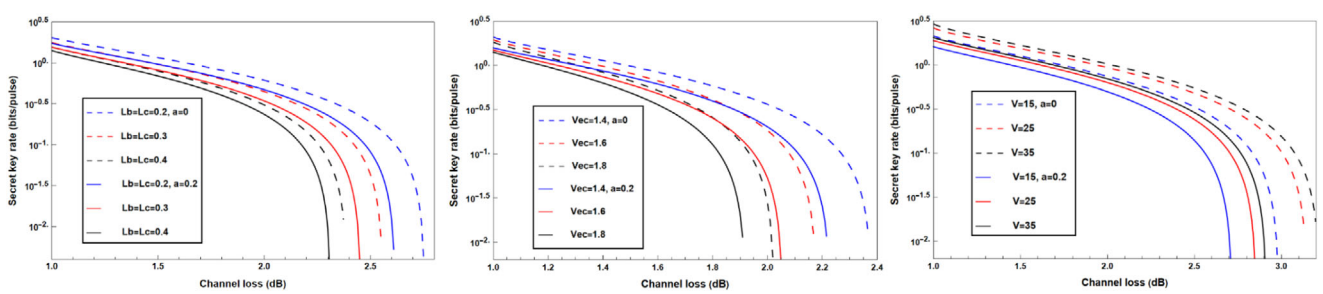

FIGURE 8 | Variations of key rate with different influencing factors under entanglement attack. The dashed line corresponds to $\mathcal{A} = 0.0$ and the solid line to $\mathcal{A} = 0.2$. In the left subplot, the blue line represents $L_B = L_C = 0.2$, the red line denotes $L_B = L_C = 0.3$, and the black line indicates $L_B = L_C = 0.4$ with other parameters set as $V = 30$ and $V_{E_A} = V_{E_B} = V_{E_C} = 1.07$; the middle subplot shows the blue line corresponding to $V_{E_C} = 1.4$, the red line to $V_{E_C} = 1.6$, and the black line to $V_{E_C} = 1.8$ with other parameters set as $V = 25$ and $L_B = L_C = 0.15$; the right subplot presents the blue line representing $V = 15$, the red line denoting $V = 25$, and the black line indicating $V = 30$ with other parameters set as $V_{E_A} = V_{E_B} = V_{E_C} = 1.03$ and $L_B = L_C = 0.1$.

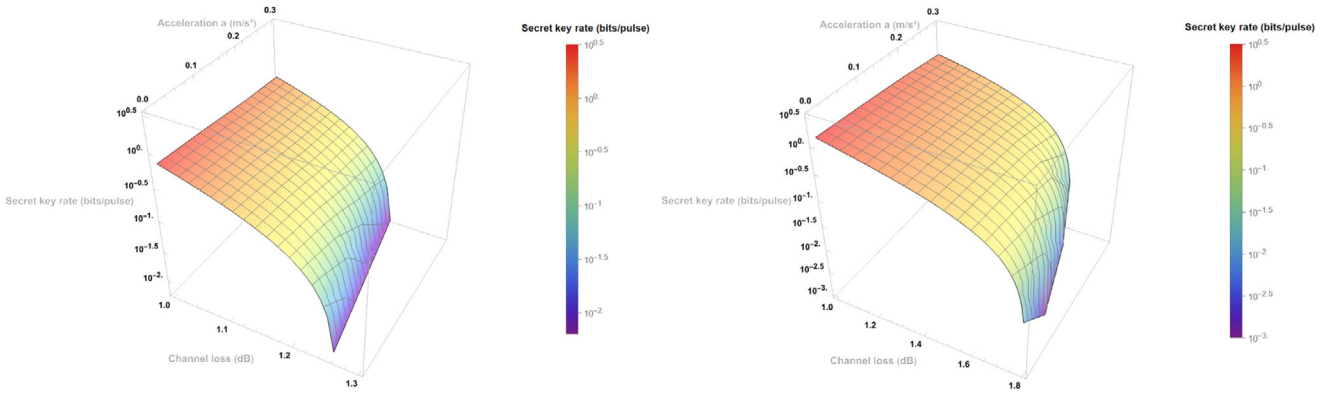

FIGURE 9 | Variations of key rate and channel loss with acceleration. The left panel corresponds to the maximum entanglement attack with $g_1 = -\sqrt{3/2}$, $g_3 = 0$, and the right panel to the independent attack with $g_1 = g_3 = 0$. Other parameter settings: $V = 30$, $V_{E_A} = V_{E_B} = V_{E_C} = 2$, and $L_B = L_C = 0.3$.

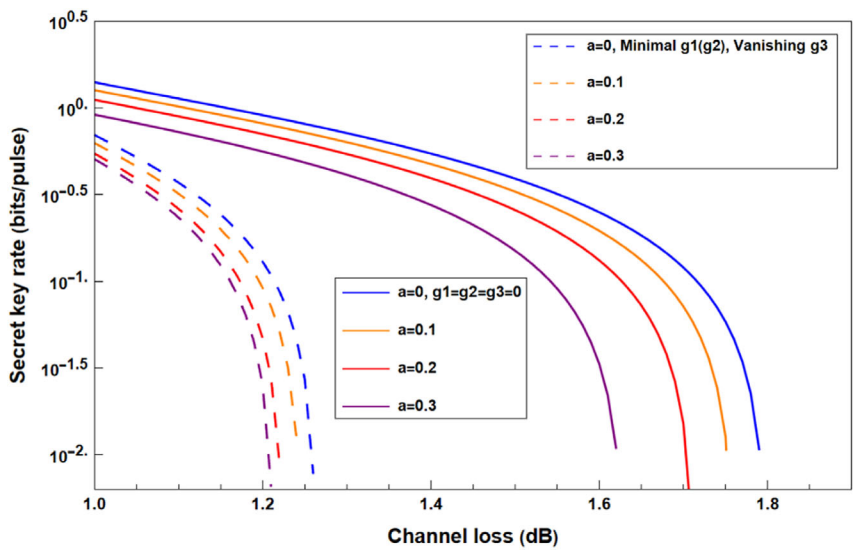

FIGURE 10 | Variations of key rate with acceleration for maximum entanglement attacks and independent attacks. The dashed line corresponds to the maximum entanglement attack with $g_1 = -\sqrt{3/2}$ and $g_3 = 0$; the solid line corresponds to the independent attack with $g_1 = g_3 = 0$. The blue line represents $\mathcal{A} = 0.0$, the orange line $\mathcal{A} = 0.1$, the red line $\mathcal{A} = 0.2$, and the purple line $\mathcal{A} = 0.3$.

entanglement attacks and independent attacks. As acceleration increases, both the key rate and transmission distance are impaired. To observe the impact of acceleration on these two types of attacks in greater detail, Figure 10 presents the two-dimensional planar graphs of the attacks. It can be observed that under maximum entanglement attacks, the attenuation degree of the key rate gradually increases as the acceleration rises to the same extent; whereas under independent attacks, the attenuation degree of the key rate gradually weakens as the acceleration increases to the same extent. This is mainly because the two types of attacks correspond to different initial correlation structures. In entanglement attacks, the noise injected by the adversary (Eve) into the channels of each communicating party is mutually correlated. Therefore, acceleration acts on the entire multimode correlation structure. It not only weakens the effective correlations among legitimate communicating parties, but also further disturbs the original balance between the eavesdropper's correlated noise and the legitimate correlations, making the multiparty correlation structure more vulnerable to destruction under relatively large acceleration. Meanwhile, the thermal noise induced by acceleration increases as the acceleration grows. Consequently, the same magnitude of acceleration increment leads to a more pronounced degradation of the key rate. In independent attacks, the noise injected by the eavesdropper (Eve) into the channels of each communicating party is mutually independent. Acceleration serves to weaken the useful correlations among legitimate communicating parties and increase local thermal noise. Once acceleration has weakened the correlations among communicating parties to a low level, further increasing the acceleration will only disrupt a limited amount of useful correlations. Therefore, the degradation of the key rate gradually diminishes.

5.2 | Quantum Secret Sharing

This section investigates the influence of different accelerations on the secure communication key in QSS under the scenario where Eve launches an attack against Alice and Bob. It is assumed

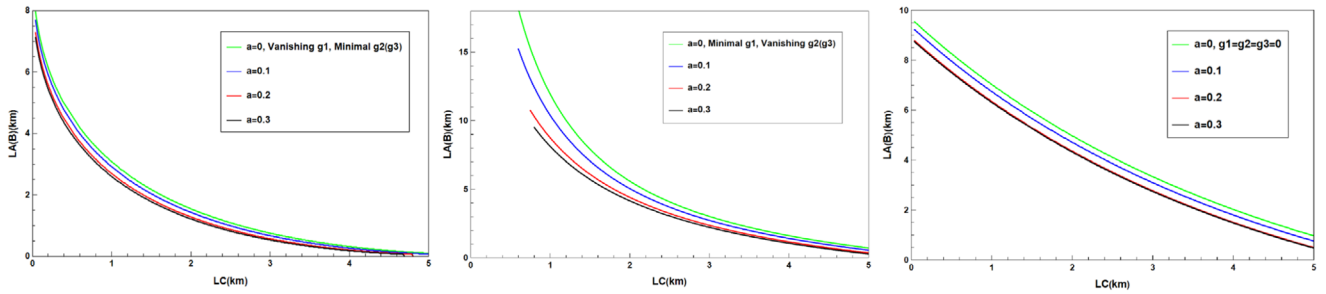

FIGURE 11 | The variation of the maximum transmission distance with acceleration. The green curve corresponds to $\mathcal{A} = 0$, the blue curve to $\mathcal{A} = 0.1$, the red curve to $\mathcal{A} = 0.2$, and the black curve to $\mathcal{A} = 0.3$. The left subplot depicts the maximum entanglement attack scenario where $g_1 = 0$ and $g_2 = -\sqrt{\frac{3}{2}}$. The middle subplot corresponds to the maximum entanglement attack scenario where $g_1 = -\sqrt{3}$ and $g_2 = 0$. The right subplot represents the independent attack scenario with $g_1 = g_2 = 0$. Other parameter settings: $V = 20$, $V_{E_A} = V_{E_B} = V_{E_C} = 2$, $L_A = L_B \neq L_C$, $\eta_{A(B,C)} = 10^{-\frac{L_{A(B,C)}}{10}}$.

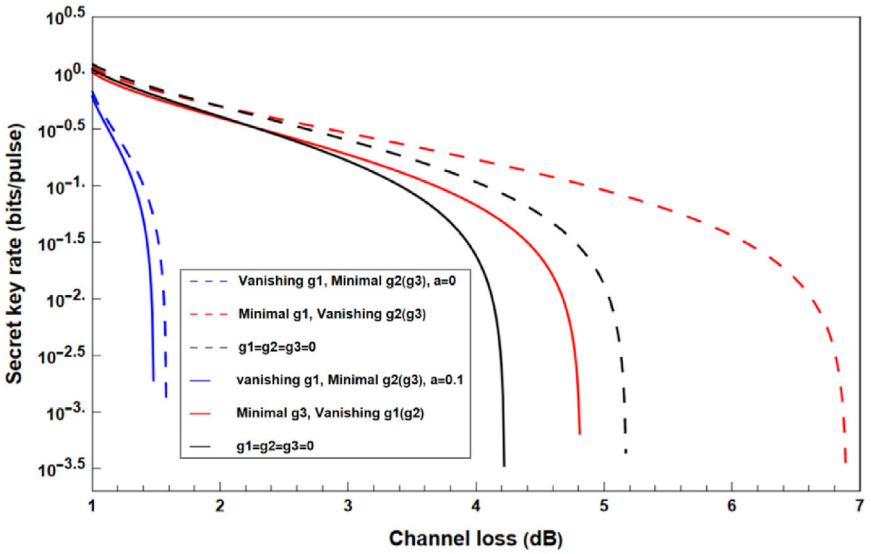

FIGURE 12 | The effect of acceleration on two types of maximum entanglement attacks and the independent attack. The dashed line corresponds to $\mathcal{A} = 0$. The solid line corresponds to $\mathcal{A} = 0.1$. The blue line corresponds to the case with $g_1 = 0$ and $g_2 = -\sqrt{3/2}$, the red line to the maximum entanglement attack with $g_1 = -\sqrt{V_{E_C}^2 - 1}$ and $g_2 = 0$, and the black line to the independent attack. Other parameter settings: $V = 20$, $V_{E_A} = V_{E_B} = V_{E_C} = 2$, $L_B = L_C = 0.3$.

that the attacks on the channels of Alice and Bob are identical, i.e., satisfying the conditions $V_{E_A} = V_{E_B}$ and $g_2 = g_3$.

Figure 11 illustrates the variation of the maximum communication distance when $K_{\mathrm{QSS}}^{\mathrm{RR}} > 0$ with increasing acceleration. It is evident that the maximum communication distance gradually decreases as acceleration increases.

Figure 13 illustrates the effect of acceleration on the two types of maximum entanglement attacks and the independent attack. It can be observed that when the channel loss is approximately 2 dB, the key rate under the independent attack begins to be lower than that of the entanglement attack with $g_1 = -\sqrt{3}$ and $g_2 = 0$. Additionally, as shown in Figure 11, when $L_A \approx 2$, the maximum transmission distance of this entanglement attack also becomes smaller than that of the independent attack. While the secure key rates of all attacks are attenuated, it is also noted that the attenuation degrees of both the maximum entanglement attack with $g_1 = 0$ and $g_2 = -\sqrt{3/2}$ and the independent attack are smaller than that of the entanglement attack with $g_1 = -\sqrt{3}$ and $g_2 = 0$.

Figure 12 illustrates the effect of acceleration on the variation of each parameter under the entanglement attack with $g_1 = 0$ and $g_2 = -\sqrt{(V_{E_C}^2 - 1)/2}$. It can be observed that acceleration only weakens the key rate, and its influence on each parameter is consistent with the variation trend in the inertial frame.

Figure 14 illustrates the effect of acceleration on the key rate under the second type of maximum entanglement attack with $g_1 = -\sqrt{(V_{E_C}^2 - 1)}$ and $g_2 = 0$. As acceleration increases, the key rate decreases progressively, but the effect of the same acceleration increment becomes increasingly less significant, and its overall trend is similar to that of the first type of maximum entanglement attack.

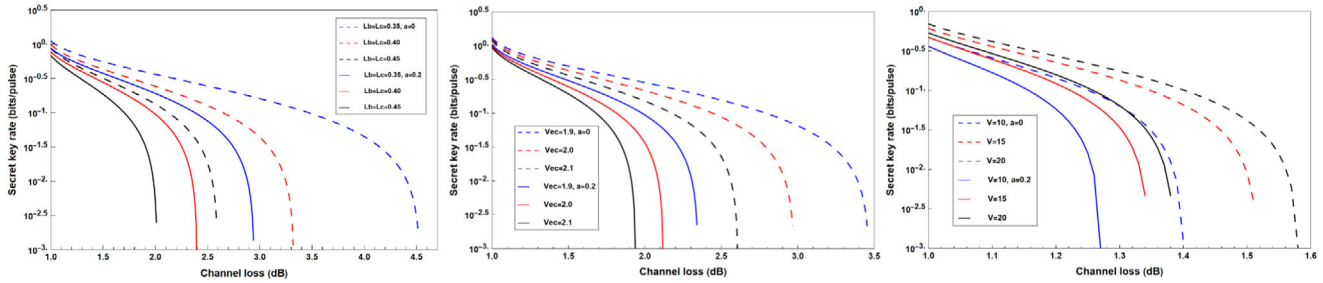

FIGURE 13 | Variations of key rate with different influencing factors under entanglement attack. The dashed line corresponds to $\mathcal{A} = 0.0$ and the solid line to $\mathcal{A} = 0.2$. In the left subplot, the blue line represents $L_B = L_C = 0.35$, the red line denotes $L_B = L_C = 0.40$, and the black line indicates $L_B = L_C = 0.45$ with other parameters set as $V = 20$ and $V_{E_A} = V_{E_B} = V_{E_C} = 1.3$; the middle subplot shows the blue line corresponding to $V_{E_C} = 1.9$, the red line to $V_{E_C} = 2.0$, and the black line to $V_{E_C} = 2.1$ with other parameters set as $V = 20$ and $L_B = L_C = 0.2$; the right subplot presents the blue line representing $V = 10$, the red line denoting $V = 15$, and the black line indicating $V = 20$ with other parameters set as $V_{E_A} = V_{E_B} = V_{E_C} = 2$ and $L_B = L_C = 0.3$.

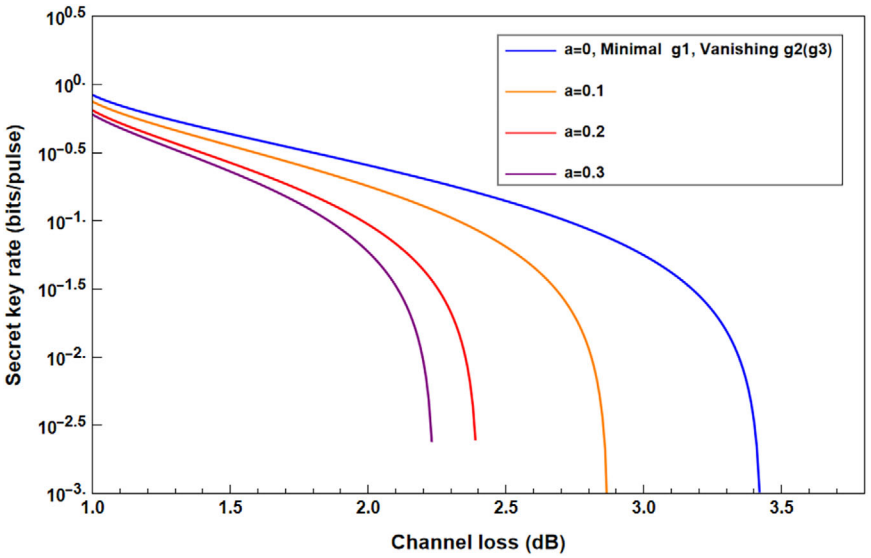

FIGURE 14 | The effect of acceleration on the key rate under maximum entanglement attacks. The blue line represents $\mathcal{A} = 0.0$, the orange line $\mathcal{A} = 0.1$, the red line $\mathcal{A} = 0.2$, and the purple line $\mathcal{A} = 0.3$. Other parameters are set as follows: $V = 20$, $V_{E_A} = V_{E_B} = V_{E_C} = 2$, $L_B = L_C = 0.4$.

6 | Conclusion

This study proposes a scalable method for analyzing the impact of gravity on CV multiparty quantum communication. When communicating parties are in accelerated motion, the performance of all protocols exhibits a downward trend. Nevertheless, several key findings merit particular attention, as they clearly reveal significant correlations between gravitational effects and different multiparty quantum communication protocols as well as their associated system configurations.

Our results demonstrate that the strength of gravitational effects on the security performance of QCC is significantly weaker than their impact on the security performance of QSS. Increasing acceleration leads to varying degrees of reduction in the maximum communication distance with a positive key rate for both protocols. Acceleration degrades the key rate as a result of mode transformations in non-inertial reference frames. This results in mode mismatch between accelerated wave packets and inertial wave packets, which breaks the correlations among communicating parties in CV GHZ states and converts vacuum fluctuations into thermal noise. Such decoherence and thermal noise induced by acceleration diminish the mutual information among legitimate communication parties and extend the information limit that eavesdropper Eve can intercept. When the acceleration of the three communicating parties remains constant, the key rate of the protocol is negatively correlated with the distance between the three parties and the thermal noise injected by the eavesdropper into the corresponding channels, while it is positively correlated with the variance of the tripartite two-mode squeezed states. This trend is entirely consistent with the laws in inertial frames, where acceleration only serves to weaken the key rate. It follows that, although gravitational effects exert corrections on the equations of quantum field theory, they do not bring about fundamental alterations to the laws in inertial frames.

The method proposed in this paper for analyzing the impact of acceleration on multiparty quantum information protocols can be further extended to accelerated scenarios with a higher number

of modes. However, it should be noted that, consistent with previous studies, this work also neglects some of the higher-order expansion terms of the Bogoliubov coefficients and fails to take into account the relevant effects induced by $\beta_{ij}^{(2)}$. For gravitational influence scenarios involving more modes, it is inevitable to incorporate the higher-order expansion of the Bogoliubov coefficients into the computational model. This research avenue is not only a priority for our future endeavors but also a highly challenging undertaking.

Acknowledgements

This work was supported by the Quantum Science and Technology-National Science and Technology Major Project (Grant No.2021ZD0300700), the National Natural Science Foundation of China grant numbers 62272483, the Open Project Program of the SJTU Pinghu Institute of Intelligent Optoelectronics Grant No.2022SPIOE204, and the Youth Foundation of the Natural Science Foundation of Hunan Province, China (Grant No.2025JJ60411).

Conflicts of Interest

The authors declare no conflicts of interest.

Data Availability Statement

The data that support the findings of this study are available from the corresponding author upon reasonable request.

References

1. M. Smania, A. M. Elhassan, A. Tavakoli, and M. Bourennane, "Experimental Quantum Multiparty Communication Protocols," *npj Quantum Information* 2 (2016): 16010.

2. A. Pandit, "Quantum Advantages in Multiparty Communication," (2025), arXiv:2512.05538 [quant-ph].

3. S. Bose, V. Vedral, and P. L. Knight, "Multiparticle Generalization of Entanglement Swapping," *Physical Review A* 57 (1998): 822.

4. M. Hillery, V. Bužek, and A. Berthiaume, "Quantum secret sharing," *Physical Review A* 59 (1999): 1829.

5. Z.-J. Zhang, Y. Li, and Z.-X. Man, "Multiparty Quantum Secret Sharing," *Physical Review A* 71 (2005): 044301.

6. V. C. Usenko, A. Acín, R. Alléaume, et al., "Continuous-Variable Quantum Communication," (2025), arXiv:2501.12801.

7. A. Saxena, K. Thapliyal, and A. Pathak, "Continuous Variable Controlled Quantum Dialogue and Secure Multiparty Quantum Computation," *International Journal of Quantum Information* 18 (2020): 2050009.

8. Y. Tian, P. Wang, J. Liu, et al., "Experimental Demonstration of Continuous-Variable Measurement-Device-Independent Quantum Key Distribution Over Optical Fiber," *Optica* 9, no. 5 (2022): 492–500.

9. G.-J. Fan-Yuan, F.-Y. Lu, S. Wang, et al., "Measurement-Device-Independent Quantum Key Distribution for Nonstandalone Networks," *Photonics Research* 9 (2021): 1881.

10. J. Li, W. Wang, and H.-K. Lo, "Fully Passive Measurement-Device-Independent Quantum Key Distribution," *Physical Review Applied* 21 (2024): 064056.

11. R. Zhao, J. Zhou, R. Shi, et al., "Continuous-Variable Measurement-Device-Independent Multipartite Quantum Communication via a Fast-Fading Channel," *Physical Review A* 111 (2025): 012613.

12. Y. Wu, J. Zhou, X. Gong, et al., "Continuous-Variable Measurement-Device-Independent Multipartite Quantum Communication," *Physical Review A* 93 (2016): 022325.

13. J. Fu, B. Su, J. Zhou, et al., "Four-State Continuous Variable Quantum Key Distribution With Two Accelerating Partners," *Physics Letters A* 501 (2024): 129399.

14. Y. Zhang, J. Fu, J. Zhou, et al., "Effects of Gravity on Passive-State Continuous Variable Quantum Key Distribution," *Annals of Physics* 477 (2025): 170003.

15. L. X. Wu, Y. Y. Feng, J. Zhou, et al., "The Effect of Acceleration on Continuous-Variable Quantum Key Distribution With Discrete Modulation," *European Physical Journal Plus* 138 (2023): 963.

16. D. E. Bruschi, T. C. Ralph, I. Fuentes, et al., "Spacetime Effects on Satellite-Based Quantum Communications," *Physical Review D* 90 (2014): 045041.

17. T. Liu, S. Wu, and S. Cao, "The Influence of the Earth's Curved Spacetime on Gaussian Quantum Coherence," *Laser Physics Letters* 16 (2019): 095201.

18. L. C. B. Crispino, A. Higuchi, and G. E. A. Matsas, "The Unruh Effect and Its Applications," *Reviews of Modern Physics* 80 (2008): 787.

19. B. Richter, K. Lorek, A. Dragan, and Y. Omar, "Effect of Acceleration on Localized Fermionic Gaussian States: From Vacuum Entanglement to Maximally Entangled States," *Physical Review D* 95 (2017): 076004.

20. P. T. Grochowski, G. Rajchel, F. Kiałka, and A. Dragan, "Effect of Relativistic Acceleration on Continuous Variable Quantum Teleportation and Dense Coding," *Physical Review D* 95 (2017): 105005.

21. M. Ahmadi, K. Lorek, A. Chęcińska, et al., "Effect of Relativistic Acceleration on Localized Two-Mode Gaussian Quantum States," *Physical Review D* 93 (2016): 124031.

22. J. Zhou, R. Shi, and Y. Guo, "Squeezed-State Quantum Key Distribution With a Rindler Observer," *Quantum Information Processing* 17 (2018): 47.

23. T. C. Ralph and N. Walk, "Quantum Key Distribution Without Sending a Quantum Signal," *New Journal of Physics* 17 (2015): 063008.

24. R. Pierini, "Effects of Gravity on Continuous-Variable Quantum Key Distribution," *Physical Review D* 98 (2018): 125007.

25. J. Zhang and S. L. Braunstein, "Continuous-Variable Gaussian Analog of Cluster States," *Physical Review A* 73 (2006): 032318.

26. Y.-H. Zhou, S.-F. Qin, W.-M. Shi, and Y.-G. Yang, "Measurement-Device-Independent Continuous Variable Semi-Quantum Key Distribution Protocol," *Quantum Information Processing* 21 (2022): 303.

27. U. H. Gerlach, "Quantum States of a Field Partitioned by an Accelerated Frame," *Physical Review D* 40 (1989): 1037.

28. A. Dragan, J. Doukas, E. Martín-Martínez, and D. E. Bruschi, "Localized Projective Measurement of a Quantum Field in Non-Inertial Frames," *Classical and Quantum Gravity* 30 (2013): 235006.

29. A. Ali, S. Al-Kuwari, M. Ghominejad, et al., "Quantum Characteristics Near Event Horizons," *Physical Review D* 110 (2024): 064001.

30. A. Dragan, I. Fuentes, and J. Louko, "Quantum Accelerometer: Distinguishing Inertial Bob From His Accelerated Twin Rob by a Local Measurement," *Physical Review D* 83 (2011): 085020.

31. M. Ahmadi, Y.-D. Wu, and B. C. Sanders, "Relativistic (2,3)-Threshold Quantum Secret Sharing," *Physical Review D* 96 (2017): 065018.

32. T. R. Perche, "Closed-Form Expressions For Smeared Bidistributions of a Massless Scalar Field: Nonperturbative and Asymptotic Results in Relativistic Quantum Information," *Physical Review D* 110 (2024): 025013.

33. G. Adesso, S. Ragy, and A. R. Lee, "Continuous Variable Quantum Information: Gaussian States and Beyond," *Open Systems and Information Dynamics* 21 (2014): 1440001.

34. M. de Gosson and F. Luef, "Symplectic Capacities and the Geometry of Uncertainty: The Irruption of Symplectic Topology in Classical and Quantum Mechanics," *Physics Reports* 484 (2009): 131.

35. M. Kasprzak and E. Tjoa, "Transmission of Quantum Information Through Quantum Fields in Curved Spacetimes," *Journal of Physics A: Mathematical and Theoretical* 58 (2025): 095301.

36. N. F. Del Grosso, F. C. Lombardo, and P. I. Villar, "Entanglement Degradation of Cavity Modes Due to The Dynamical Casimir Effect," *Physical Review D* 102 (2020): 125008.

37. C. J. Fewster, D. W. Janssen, L. D. Loveridge, et al., "Quantum Reference Frames, Measurement Schemes and the Type of Local Algebras in Quantum Field Theory," *Communications in Mathematical Physics* 406 (2024): 19.

38. M. Ahmadi, D. E. Bruschi, C. Sabín, et al., "Relativistic Quantum Metrology: Exploiting relativity to Improve Quantum Measurement Technologies," *Scientific Reports* 4 (2014): 4996.

39. Y. Zhou, J. Yu, Z. Yan, et al., "Quantum Secret Sharing Among Four Players Using Multipartite Bound Entanglement of an Optical Field," *Physical Review Letters* 121 (2018): 150502.

40. Y. Qin, J. Cheng, J. Ma, et al., "Efficient and Secure Quantum Secret Sharing For Eight Users," *Physical Review Research* 6 (2024): 033036.

Appendix A

Parameter Calculation Process: First, a 6×6 covariance matrix for thermal noise injected by Eve into three channels is constructed. Subsequently, specific operations are performed between this matrix and the matrices established by three legitimate parties to obtain the covariance matrix of the entire system, denoted as $V_{A,B,C,\mathrm{Eve}}$. The system matrix is rearranged in the order of A, E_A, B, E_B, C, E_C, followed by the transformation operation $\mathbf{U}_{\mathrm{David}}\mathbf{U}_{\mathrm{Eve}}\mathbf{V}_{A,E_A,B,E_B,C,E_C}\mathbf{U}_{\mathrm{Eve}}^{T}\mathbf{U}_{\mathrm{David}}^{T}$ using the beam splitter matrices $\mathbf{U}_{\mathrm{David}}$ and $\mathbf{U}_{Eve}$ with specific rows and columns removed. After that, the modes are rearranged in the order of A_1, B_1, C_1, D, E, F to derive the covariance matrix $\mathbf{V}_{A_1,B_1,C_1,D,E,F}$. Finally, the multiparty quantum communication matrix ($\mathbf{V}_{A_1,B_1,C_3|\hat{X}_D,\hat{X}_E,\hat{P}_F}$) is obtained through partial homodyne measurement and iterative operations.

For parameter A:

$$A = V_a + \frac{U_2}{U_1} - \frac{U_3\cdot U_4^2}{U_1^2\left(U_5 - \frac{U_6^2}{U_1}\right)} \tag{A1}$$

where

$$\begin{aligned}
U_1 &= 2g_1\sqrt{1-t_a}\sqrt{1-t_b} - 4g_2\sqrt{1-t_a}\sqrt{1-t_c} - 4g_3\sqrt{1-t_b}\sqrt{1-t_c}\\
&\quad + t_aV_a + t_bV_a + 4t_cV_a + V_{ea} - t_aV_{ea} + V_{eb} - t_bV_{eb} + 4V_{ec}\\
&\quad - 4t_cV_{ec},\\
U_2 &= t_a - t_aV_a^2,\\
U_3 &= 4t_a(-1+V_a^2),\\
U_4 &= g_1\sqrt{1-t_a}\sqrt{1-t_b} - g_2\sqrt{1-t_a}\sqrt{1-t_c} - 3g_3\sqrt{1-t_b}\sqrt{1-t_c}\\
&\quad + t_bV_a + 2t_cV_a + V_{eb} - t_bV_{eb} + 2V_{ec} - 2t_cV_{ec},\\
U_5 &= -2g_1\sqrt{1-t_a}\sqrt{1-t_b} + t_bV_a + t_a(V_a - V_{ea}) + V_{ea} + V_{eb} - t_bV_{eb},\\
U_6 &= 2g_2\sqrt{1-t_a}\sqrt{1-t_c} - 2g_3\sqrt{1-t_b}\sqrt{1-t_c} - t_aV_a + t_bV_a - V_{ea}\\
&\quad + t_aV_{ea} + V_{eb} - t_bV_{eb}.
\end{aligned}$$

For parameter B:

$$B = \frac{U_1\cdot U_2}{U_3} \tag{A2}$$

where

$$\begin{aligned}
U_1 &= \sqrt{t_a}\sqrt{t_b}(-1+V_a^2),\\
U_2 &= g_1\sqrt{1-t_a}\sqrt{1-t_b} - g_2\sqrt{1-t_a}\sqrt{1-t_c} - g_3\sqrt{1-t_b}\sqrt{1-t_c}\\
&\quad + t_cV_a + V_{ec} - t_cV_{ec},\\
U_3 &= -g_3^2 + g_3^2t_b + g_1^2(-1+t_a+t_b-t_at_b) + g_3^2t_c - g_3^2t_bt_c\\
&\quad + g_2^2(-1+t_a+t_c-t_at_c) - 2g_3t_a\sqrt{1-t_b}\sqrt{1-t_c}V_a + t_at_bV_a^2\\
&\quad + t_at_cV_a^2 + t_bt_cV_a^2 - 2g_3\sqrt{1-t_b}\sqrt{1-t_c}V_{ea}\\
&\quad + 2g_3t_a\sqrt{1-t_b}\sqrt{1-t_c}V_{ea} + t_bV_aV_{ea} - t_at_bV_aV_{ea} + t_cV_aV_{ea}\\
&\quad - t_at_cV_aV_{ea} + t_aV_aV_{eb} - t_at_bV_aV_{eb} + t_cV_aV_{eb} - t_bt_cV_aV_{eb}\\
&\quad + V_{ea}V_{eb} - t_aV_{ea}V_{eb} - t_bV_{ea}V_{eb} + t_at_bV_{ea}V_{eb}\\
&\quad - 2g_2\sqrt{1-t_a}(g_3\sqrt{1-t_b}(-1+t_c) + \sqrt{1-t_c}(t_bV_a + V_{eb}\\
&\quad - t_bV_{eb})) + t_aV_aV_{ec} + t_bV_aV_{ec} - t_at_cV_aV_{ec} - t_bt_cV_aV_{ec}\\
&\quad + V_{ea}V_{ec} - t_aV_{ea}V_{ec} - t_cV_{ea}V_{ec} + t_at_cV_{ea}V_{ec} + V_{eb}V_{ec}\\
&\quad - t_bV_{eb}V_{ec} - t_cV_{eb}V_{ec} + t_bt_cV_{eb}V_{ec} - 2g_1(g_3\sqrt{1-t_a}\\
&\quad \times(-1+t_b)\sqrt{1-t_c} + \sqrt{1-t_b}(g_2(-1+t_a)\sqrt{1-t_c}\\
&\quad + \sqrt{1-t_a}(t_cV_a + V_{ec} - t_cV_{ec}))).
\end{aligned}$$

For parameter C:

$$C = V_a - \frac{U_1}{U_2+U_3} \tag{A3}$$

where

$$\begin{aligned}
U_1 &= t_a(-1+V_a^2),\\
U_2 &= -2g_1\sqrt{1-t_a}\sqrt{1-t_b} - 2g_2\sqrt{1-t_a}\sqrt{1-t_c} - 2g_3\sqrt{1-t_b}\sqrt{1-t_c}\\
U_3 &= t_aV_a + t_bV_a + t_cV_a + V_{ea} - t_aV_{ea} + V_{eb} - t_bV_{eb} + V_{ec} - t_cV_{ec}.
\end{aligned}$$

For parameter D:

$$D = -\frac{U_1}{U_2} \tag{A4}$$

where

$$\begin{aligned}
U_1 &= \sqrt{t_a}\sqrt{t_b}(-1+V_a^2),\\
U_2 &= -2g_1\sqrt{1-t_a}\sqrt{1-t_b} - 2g_2\sqrt{1-t_a}\sqrt{1-t_c} - 2g_3\sqrt{1-t_b}\sqrt{1-t_c}\\
&\quad + t_aV_a + t_bV_a + t_cV_a + V_{ea} - t_aV_{ea} + V_{eb} - t_bV_{eb} + V_{ec} - t_cV_{ec}.
\end{aligned}$$

For parameter E:

$$E = V_a + \frac{U_2}{U_1} - \frac{U_3\cdot U_4^2}{U_1^2\left(U_5 - \frac{U_6^2}{U_1}\right)} \tag{A5}$$

where

$$\begin{aligned}
U_1 &= 2g_1\sqrt{1-t_a}\sqrt{1-t_b} - 4g_2\sqrt{1-t_a}\sqrt{1-t_c} - 4g_3\sqrt{1-t_b}\sqrt{1-t_c}\\
&\quad + t_aV_a + t_bV_a + 4t_cV_a + V_{ea} - t_aV_{ea} + V_{eb} - t_bV_{eb} + 4V_{ec}\\
&\quad - 4t_cV_{ec},\\
U_2 &= t_b - t_bV_a^2,\\
U_3 &= 4t_b(-1+V_a^2),\\
U_4 &= g_1\sqrt{1-t_a}\sqrt{1-t_b} - 3g_2\sqrt{1-t_a}\sqrt{1-t_c} - g_3\sqrt{1-t_b}\sqrt{1-t_c}\\
&\quad + t_aV_a + 2t_cV_a + V_{ea} - t_aV_{ea} + 2V_{ec} - 2t_cV_{ec},\\
U_5 &= -2g_1\sqrt{1-t_a}\sqrt{1-t_b} + t_bV_a + t_a(V_a - V_{ea}) + V_{ea} + V_{eb} - t_bV_{eb},\\
U_6 &= 2g_2\sqrt{1-t_a}\sqrt{1-t_c} - 2g_3\sqrt{1-t_b}\sqrt{1-t_c} - t_aV_a + t_bV_a - V_{ea}\\
&\quad + t_aV_{ea} + V_{eb} - t_bV_{eb}.
\end{aligned}$$

For parameter F:

$$F = \frac{U_1\cdot U_2}{U_3} \tag{A6}$$

where

$$\begin{aligned}
U_1 &= \sqrt{t_b}\sqrt{t_c}(-1+V_a^2),\\
U_2 &= -g_1\sqrt{1-t_a}\sqrt{1-t_b} - g_2\sqrt{1-t_a}\sqrt{1-t_c} + g_3\sqrt{1-t_b}\sqrt{1-t_c}\\
&\quad + t_aV_a + V_{ea} - t_aV_{ea},\\
U_3 &= -g_3^2 + g_3^2t_b + g_1^2(-1+t_a+t_b-t_at_b) + g_3^2t_c - g_3^2t_bt_c\\
&\quad + g_2^2(-1+t_a+t_c-t_at_c) - 2g_3t_a\sqrt{1-t_b}\sqrt{1-t_c}V_a + t_at_bV_a^2\\
&\quad + t_at_cV_a^2 + t_bt_cV_a^2 - 2g_3\sqrt{1-t_b}\sqrt{1-t_c}V_{ea}\\
&\quad + 2g_3t_a\sqrt{1-t_b}\sqrt{1-t_c}V_{ea} + t_bV_aV_{ea} - t_at_bV_aV_{ea} + t_cV_aV_{ea}\\
&\quad - t_at_cV_aV_{ea} + t_aV_aV_{eb} - t_at_bV_aV_{eb} + t_cV_aV_{eb} - t_bt_cV_aV_{eb}\\
&\quad + V_{ea}V_{eb} - t_aV_{ea}V_{eb} - t_bV_{ea}V_{eb} + t_at_bV_{ea}V_{eb} - 2g_2\sqrt{1-t_a}\\
&\quad \times(g_3\sqrt{1-t_b}(-1+t_c) + \sqrt{1-t_c}(t_bV_a + V_{eb} - t_bV_{eb}))\\
&\quad + t_aV_aV_{ec} + t_bV_aV_{ec} - t_at_cV_aV_{ec} - t_bt_cV_aV_{ec} + V_{ea}V_{ec}\\
&\quad - t_aV_{ea}V_{ec} - t_cV_{ea}V_{ec} + t_at_cV_{ea}V_{ec} + V_{eb}V_{ec} - t_bV_{eb}V_{ec}
\end{aligned}$$

$$- t_c V_{eb} V_{ec} + t_b t_c V_{eb} V_{ec} - 2g_1(g_3\sqrt{1-t_a}(-1+t_b)\sqrt{1-t_c} + \sqrt{1-t_b}(g_2(-1+t_a)\sqrt{1-t_c} + \sqrt{1-t_a}(t_c V_a + V_{ec} - t_c V_{ec}))).$$

For parameter G:

$$G = V_a - \frac{U_1}{U_2} \tag{A7}$$

where

$$U_1 = t_b(-1+V_a^2),$$

$$U_2 = -2g_1\sqrt{1-t_a}\sqrt{1-t_b} - 2g_2\sqrt{1-t_a}\sqrt{1-t_c} - 2g_3\sqrt{1-t_b}\sqrt{1-t_c} + t_a V_a + t_b V_a + t_c V_a + V_{ea} - t_a V_{ea} + V_{eb} - t_b V_{eb} + V_{ec} - t_c V_{ec}.$$

For parameter H:

$$H = -\frac{U_1}{U_2} \tag{A8}$$

where

$$U_1 = \sqrt{t_b}\sqrt{t_c}(-1+V_a^2),$$

$$U_2 = -2g_1\sqrt{1-t_a}\sqrt{1-t_b} - 2g_2\sqrt{1-t_a}\sqrt{1-t_c} - 2g_3\sqrt{1-t_b}\sqrt{1-t_c} + t_a V_a + t_b V_a + t_c V_a + V_{ea} - t_a V_{ea} + V_{eb} - t_b V_{eb} + V_{ec} - t_c V_{ec}.$$